Mou, Z., Triantis, I., Woods, V. M., Toumazou, C. & Nikolic, K. (2012). A simulation study of the combined thermoelectric extracellular stimulation of the sciatic nerve of the Xenopus laevis: the localized transient heat block. IEEE Transactions on Biomedical Engineering, 59(6), pp. 1758-1769. doi: 10.1109/TBME.2012.2194146

A Simulation Study of the Combined Thermoelectric Extracellular Stimulation of the Sciatic Nerve of the *Xenopus Laevis*: the Localized Transient Heat Block

Zongxia Mou, Iasonas F. Triantis, Member, IEEE, Virginia M. Woods, Student Member, IEEE, Christofer Toumazou, Fellow IEEE, and Konstantin Nikolic, Member, IEEE

Abstract—This paper presents the response of the Xenopus laevis nerve fibers to combinations of electrical (cuff electrodes) and optical (infrared laser, low power sub-5mW) stimulation. Assuming that the main effect of the laser irradiation on the nerve tissue is the localized temperature increase, this paper analyzes and gives new insights into the function of the combined thermoelectric stimulation on both excitation and blocking of the nerve action potentials (AP). The calculations involve a finite-element model (COMSOL) to represent the electrical properties of the nerve and cuff. Electric field distribution along the nerve was computed for the given stimulation current profile and imported into a NEURON model, which was built to simulate the electrical behavior of myelinated nerve fiber under extracellular stimulation. The main result of this study of combined thermoelectric stimulation showed that local temperature increase, for the given electric field, can create a transient block of both the generation and propagation of the APs. Some preliminary experimental data in support of this conclusion are also shown.

Index Terms—Neural engineering, extracellular stimulation, finite-element method, NEURON, thermal block

I. Introduction

Neural disorders or malfunction can cause severe medical conditions affecting the quality of life for millions of patients worldwide, with conventional drug treatment often being ineffective. Electrical stimulation of peripheral nerves has been developed in various degrees for treatment of conditions including foot drop, hand grasp, spinal cord injury, pain relief and epilepsy, to name a few [1]. Whilst in the first two applications, the stimulation is mostly employed for the activation of disabled or malfunctioning organs or muscles, the latter two involve stimulation for the purpose of blocking unwanted activity. In the case of spinal cord injury (SCI), both types of stimulation are required; e.g. bladder incontinence due to SCI required stimulation to cause bladder contraction and sphincter opening, whilst blocking unwanted neural activity between the bladder and the spine below the area of injury removes the need for rhizotomy [2]. However such nerves contain a number of fibre-groups (fascicles) that later connect to specific organs, including ones that are in no need for rehabilitative intervention. Additionally, the fibres in these fascicles can have different diameters and functionality.

A number of methods have been proposed for blocking nerve conduction typically based on electrical, chemical and/or thermal methods [3]. As with all types of electrical neural intervention, invasive techniques using intrafascicluar electrodes [4], offer better control and accuracy but ultimately damage the nerve. It is therefore very desirable to develop non-penetrating interfaces that allow fascicle as well as directional and fibre-type selectivity. The most established ones are cuff electrodes [1], with possible multi-electrode topologies for additional selectivity. Reversible blocking of nerve conduction in targeted structures can be achieved by using various stimulation schemes based on direct currents (e.g. DC monophasic waveforms [5]) or high frequency alternating currents (HFAC) [6]. Several recent studies have examined the biophysics of HFAC techniques in both myelinated and unmyelinated fibres, optimal electrode design and optimal waveforms [7-8]. In practice, conventional selectivity methods have exhibited limited success so far, as they require high stimulus currents and have a limited resolution evoking unwanted neural activity that can result in side effects, but they constantly pursue improvements [8]. Overall, neurostimulation for blocking is very desirable; either directly, to avert undesirable neural activity, or for refining the selectivity of activating stimulation methods.

Temperature-regulated neural control can be a strong candidate for blocking nerve propagation with the benefit of no direct contact between the stimulation source and the tissue, high spatial resolution, and no electrical interference to bio-recordings. However, the clinical implementation of thermal block is very challenging, as irreversible thermal ablation can occur during long-term stimulation. This has led to the consideration of multi-modal stimulus inputs for neural signal manipulation. To date, combined methods have only been employed in therapeutic applications as a compensation technique. Ackermann et al [3] investigated nerve cooling to remove an undesirable response during HFAC blocking.

Thermal neural inhibition (or "heat block") was known since the experiments of Hodgkin and Katz [9] and Huxley [10] but only for unmyelinated axons. Raminsky [11] showed reversible thermal block in demyelinated nerves between 35 and 36 °C and irreversible heating block of myelinated A and

Manuscript received May 30, 2011. This work was supported in part by the UK EPSRC grant EP/H024581. ZM would like to thank China Scholarship Council for financial support and Prof. Toumazou for the opportunity to join the Centre for Bio-Inspired Technology at Imperial College London. ZM also thanks N.T. Carnevale, from Dep. of Psychology, Yale University for his generous advice on NEURON modeling

Z.M. is with the Bioengineering College, Chongqing University, Chongqing 400044, China.

I.T. is with the Department of Electrical and Electronic Engineering, University College London, London WC1E 6EZ, UK.

V.W. and C.T. are with the Department of Electrical and Electronic Engineering and Institute of Biomedical Engineering, Imperial College London, London SW7 2AZ, UK (e-mail: c.toumazou@imperial.ac.uk)

K.N. is with the Department of Electrical and Electronic Engineering and Institute of Biomedical Engineering, Imperial College London, London SW7 2AZ, UK (tel: +44 20-7954-1594, e-mail: k.nikolic@imperial.ac.uk)

C-fibres of the cat was shown in [12]. The influence of temperature on the response of the myelinated sciatic frog's nerve was studied by Rattay and Aberham [13]. They showed how changing kinetics of the gating mechanisms of the sodium ion channels was responsible for the faster onset of APs and reduction of the AP amplitude. However, temperature was typically considered to be a global, spatially uniform parameter. In recent research an alternative method has emerged, with the use of a laser coupled to an optic fiber, offering the ability to focus light to a very narrow beam and examine the effects of local heating on the neural behavior. The assumption is that the main effect of the laser radiation on the nerve is due to water absorption of the light, heating and consequent increase of temperature. Recently it has been discovered that very short, high-energy laser pulses can activate nerves [14-17]. This technique has been further developed and a commercial illumination system for this purpose is available. However the exact mechanism of neural activation by a burst of intense laser pulses is still not fully understood [18].

Here we examine the theoretical and experimental consequences of extracellular thermoelectric stimulation on a model of the Xenopus sciatic nerve. We use a nerve cuff electrode for electrical stimulation and a laser diode coupled to an optic fiber for inducing localized thermal effects. In Sec. II and III we give a description of our model and experimental setup. Results are given in Sec. IV including a demonstration of the thermoelectric block of neural signals. Two cases of the heat block are identified: generation block – where the creation of the AP and the temperature block take place at the same node, and propagation block – when an already propagating AP is stopped due to elevated temperature of only one or several nodes along a myelinated axon. We found that much higher temperatures are needed to induce the latter. Finally, the paper concludes by assessing the merits of combined optical and electrical stimulation for advancing selectivity in peripheral neural interfacing.

II. Thermoelectric Stimulation Modeling

First it was essential to build a model of the generation and propagation of nerve impulses under combined thermoelectric stimulation. A variety of mathematical and computer models has been used to study the electrical behavior of neural myelinated fibers. The node of Ranvier membrane excitability of Xenopus laevis was first modeled by Frankenhaeuser and Huxley (FH model) [19] and implemented later by Butikoffer [20] and Dean [21]. However, this model has only a single node without considering the mutual interaction among adjacent segments of the excitable membrane. McNeal [22] implemented a myelinated fiber model describing the electrical behavior of all nodes, but it ignored the passive electrical properties of the insulating myelin sheath. FitzHugh [23] and Bostock [24] first considered the role of the myelin internode (in addition to the active nonlinear properties at the nodes). The mathematical basis for the extracellular fiber stimulation was given by Rattay [25]. The complete description of an active nerve fiber under extracellular stimulation is essential for an investigation of the thermoelectric effects on AP initiation and blocking.

NEURON software (v7.1 [26]) was used to simulate the electrical behavior of the nerve axons. We assume that the myelin sheath is a perfect insulator and incorporate the FH model at each node of Ranvier. The electric field distribution of the surrounding area of the nerve under varying extracellular electrode configurations and stimulus patterns was calculated in COMSOL® Multiphysics 3.5a. The main advantage of this framework over the other proposed models is that spatial properties of the extracellular stimulus can be selected arbitrarily, so that one can simulate a variety of electrode-neuron geometries of practical interest. Additionally, special attention is paid to the phenomenon of the influence of ambient temperature, as well as heating specific nodes, on nerve kinetics. Recently COMSOL was used for simulating a Hodgkin-Huxley model of APs in neural fibers and corresponding electric field creation in the extracellular space [27]. Some other studies on peripheral nerve electrode simulations employed Maxwell3D in combination with NEURON [28].

III. Methods

Our simulations incorporated three modeling environments. An electrode model in Simulink accounted for the electrical drop due to the electrode-electrolyte interface. The voltage representation of the current-mode stimulus was imported into a finite-element model of the cuff electrode (COMSOL). The extracellular potential along a fiber within the nerve bundle was then exported into NEURON software, where the electrical response of the neural membrane was calculated. Thermal stimulation was realized in the membrane model by defining the local temperature at every node in NEURON. A tripolar cuff was used to stimulate the sciatic nerve of a Xenopus laevis (Fig.1a,b,c). Fig.1a shows our experimental setup which was replicated for the simulation studies: a cuff electrode surrounded the sciatic nerve with a laser fiber near the position of the central cathode (Fig.1b).

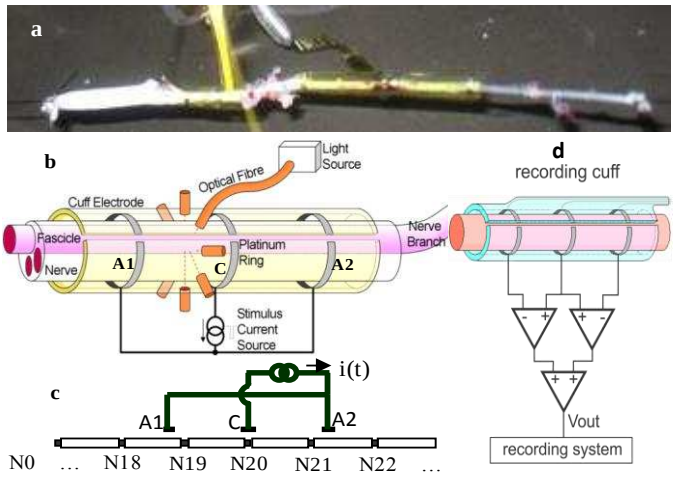

Fig. 1. (a) The cuff electrodes (provided by M. Schüettler from IMTEK, Freiburg, Germany) and the frog's sciatic nerve used in experiments and for computer simulations. The stimulation cuff is on the left hand side together with the optical fiber (vertical yellow tube) used for illuminating the nerve bundle by the laser. The recording tripolar cuff is on approximately 1cm distance to the right of the cathode electrode of the stimulation cuff and consists of three ring electrodes on 1cm distance each. (b) A schematic presentation of the nerve and stimulation tripolar cuff and the optical fiber (or several fibers), (c) cuff electrodes, the cathode (C) and two anodes (A1 and A2), stimulation current source and a myelinated axon with 41 nodes of Ranvier (labeled N0-N40). (d) The recording cuff and the amplification and recording system.

The recording cuff system with amplifiers, connected to the data acquisition system, is shown in Fig. 1d. Fig.1c shows the

concept of the stimulation system used in our simulation models. The cuff electrode was connected in a tripolar configuration and a current flowed from cathode to anode. We assumed that all the fibers are longitudinal. In our simulations we consider a myelinated fiber with 41 nodes of Ranvier (N0–N40) and 41 myelinated sections. Note that node N20 (the node where an AP was initiated), can have a variable position relative to the center of the cathode (C).

A. COMSOL model: Geometry, materials properties

A finite element model of a peripheral nerve and tripolar cuff electrode were implemented in the COMSOL simulation environment. The simulated nerve and electrode geometries, shown in Fig.2, were constructed to closely match those found in our experimental setup (see Section IIID). The starting point for the cuff model was the modeling study of the tripolar cuff electrode nerve stimulation of Goodall et.al [32]. The conductivity and dielectric permeability of each material type used in our model were found in the literature (Table 1), but the saline conductivity was obtained in our experiments to ensure the accuracy of our electrode model. Fig. 2a shows the geometry of the cuff-nerve system, vertical and radial cross sections. The z-axis (vertical axis) represents the longitudinal center line of the nerve bundle.

Fig.2b illustrates the cuff-nerve configuration within the COMSOL model. A 2D axially symmetric, homogeneous, isotropic volume conductor of the nerve was constructed in COMSOL using the conductive media AC module to solve

TABLE I
ELECTRICAL PARAMETER VALUES FOR THE MATERIAL SYSTEMS IN THE MODEL

Parameter	Contact [29]	Cuff [30]	Nerve & Epineur. [31]	Saline
Conductivity (S/m)	8.9×10^{6}	6.7×10^{-14}	0.6	0.8
Relative Permittivity	1	4	10^{5}	80

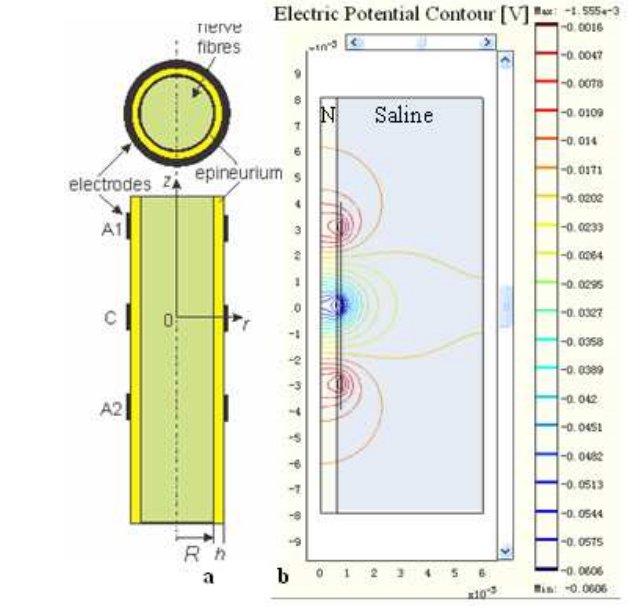

Fig. 2. (a) Cross section of the nerve and electrodes. R is the radius of the nerve bundle (R=0.6 mm, h=0.15 mm). (b) Geometry of the system used in COMSOL and the electric potential contours obtained in the simulations. Rectangle N represents the nerve bundle (0.6 x 16 mm). Rectangle Saline is the longitudinal section of the saline (6 x16 mm). A1, A2 (0.5 mm) are the anodes and C (0.5 mm) is the cathode. The metallic contacts were embedded in the polyimide substrate. The distance between cuff and nerve border is 0.15mm. The boundary conditions are described in Appendix B.

Maxwell's equations. A time-dependent solver was used in all models. Rotation of the 2D picture around the r-axis produces the 3D model of the actual cuff electrode (Fig 1a). Fig. 2b also shows the electric potential contours, a quasi static solution at the end of a stimulus pulse.

B. Electrode-electrolyte interface

The effect of the electrode-electrolyte interface was taken into consideration when calculating the potential drop across the interface during the stimulus current flow. The details of the experimental investigation of this system were reported elsewhere [33] and we only present here the equivalent circuit of the electrode-electrolyte interface (Fig.3a) and a final result (Fig.3b). We used Mathworks Simulink to simulate the equivalent circuit of the electrode-electrolyte interface and fit the parameter values given in Table 2. The stimulus current flows across the interface and the output voltages obtained in Matlab simulations were saved as a function of time into a text file. This file was then imported into the COMSOL model of a cuff-nerve system, to provide the boundary values for the electrode potentials i.e. it represents the stimulation signal. Fig. 3b gives an example of the electrical signal created after the electrode-electrolyte interface, and demonstrates the shape change of the square current pulse due to the

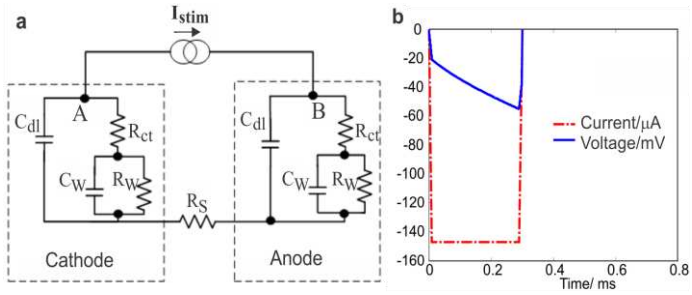

Fig. 3. (a) Equivalent circuit of the electrode-electrolyte interface. C_{dl} is the double layer capacitance, R_{ct}– charge transfer resistance, C_W – the Warburg diffusion capacitive element, R_W – the Warburg diffusion resistive element and R_S – solution bulk resistance. The Anode represents the combined impedance of both anodes. (b) Electrical stimulus signal calculated with the electrode model for square current pulse (amplitude = 147 μA, duration = 300 μs) and measured across points A and B in panel (a).

charge-discharge effect of the capacitance and resistance in the interface.

C. NEURON model

Sciatic nerve fibers of Xenopus laevis were implemented in the NEURON simulation environment [26]. Our model for the nerve fiber assumed a myelinated axon including 41 nodes of Ranvier and 41 internodes (myelin sections). The number of nodes was arbitrarily chosen with the sole purpose of having enough nodes to avoid any end effects in the simulations. The starting equation of the axon model is the classical Hodgkin-Huxley type equation [25]:

TABLE II
FITTED VALUES FOR PLATINUM BLACK-SALINE INTERFACE IN FIG. 3A

Electrode	C_{dl} (nF)	R_{ct} (Ω)	C_W (μF)	R_W (Ω)	R_S (Ω)
Cathode	1.0 k	135.3	3.98	265.7	190.8
Anode	0.5	245.1	1×10^{5}	18.99 k	

$$C_{m,n}\frac{dV_n}{dt} = -I_{ion,n} + G_{a,n+1,n}\left(V_{ext,n+1} - V_{ext,n}\right) + G_{a,n-1,n}\left(V_{ext,n-1} - V_{ext,n}\right) \quad (1)$$

TABLE III. PARAMETERS USED FOR THE FIBER MODEL

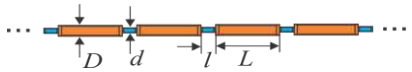

Parameter		Value		unit	Ref.
D / Fiber diameter		3-25		µm	[36]
d / Axon diameter		0.7*D		µm	[37]
L / Myelin length		100*D		µm	[38]
l / Node length		2.5		µm	
V_{rest} / Resting potential		-70		mV	
c_m / Membrane capacitance – node		2		µF/cm^2	
c_{myelin} / Membrane capacitance – myelin		0.157/(πD)		µF/cm^2	
$[Na]_{int}$ Intracellular sodium concentrati.		13.74		mM	[19] & [12]
$[Na]_{ext}$ Extracell. sodium concentration		114.5		mM	
$[K]_{int}$ Intracellular potassium concentr.		120		mM	
$[K]_{ext}$ Extracellular potassium concentr.		2.5		mM	
$\bar{P}_{Na}$ / Sodium permeability constant		8 x 10^{-3}		cm/s	
$\bar{P}_{K}$ / Potassium permeability const.		1.2 x 10^{-3}		cm/s	
$\bar{P}_{P}$ / Non-specific permeability const.		0.54 x 10^{-3}		cm/s	
g_L / Leak conductance/unit area		30.3 x 10^{-3}		mho/cm^2	
Q10 / Temperature coefficients		α	β		
	m	1.8	1.7		[34] & [12]
	h	2.8	2.9		
	n	3.2	2.8		
	p	3	3		
$Q10_\rho$ for ρ_a (axial resistivity)		1/1.3			[39]
$Q10_{ch}$ for maximum ionic conductances		1.4			
ρ_a for Temperature = 23°C (parameter adjusted to fit conduc. speed)		65		ohm·cm	[40]

$C_{m,n}$ and V_n are the membrane capacitance and the reduced membrane voltage of the n-th compartment, respectively. $V= U–V_{rest}$ where U is the absolute membrane voltage and V_{rest} is the resting voltage across the membrane. Also $U= V_{int}-V_{ext}$, where V_{int} and V_{ext} are the internal and external electrical potential of a compartment. $G_{a,,n+1,n}$ is the conductance of axoplasm between the centres of two compartments n+1 and n. Axon nodes were modeled with a single segment and the membrane kinetics at the nodes was described by the FH equations [19, 34], while each myelin section was defined as a passive electrical section and was modeled using ten compartmental segments. More details about the model are given in Appendix A. Parameters for the axon model are given in Table III along with their corresponding references.

The extracellular voltage from COMSOL (V_{ext}) was assigned to the center of each segment for every instance of time. The temperature was encoded in the model through a global parameter ('celsius'), as well as a local parameter ('localtemp') in the mod file containing a description of FH model in NMODL [35]. The local temperature was defined for each node, either as equal to 'celsius' or by assigning a specific value to it (e.g. if heated).

D. Experimental setup

The optoelectronic stimulation platform used in the experiments is shown in Fig.1.

Electrical stimulation and recording. Symmetric tripolar cuff electrodes, with 1.5 mm inner diameter and 10 mm length, were used in this experiment (Fig.1b). The cuffs were fabricated from a 5µm layer of polyimide with a 300nm layer of platinum black (IMTEK, Germany). The geometric area of each anode was 6.6 mm^2 and the total cathodal area was 1.8 mm^2. The spacing between the platinum rings was 3mm, each ring with a width of 0.5mm and the total length of the cuff was 8mm. The stimulation cuff was connected to an AC programmable current generator with a floating triax output (Keithley® 6221), which was controlled by a PC. The recording cuff was connected to the in-house built amplification system [41] and data was collected at 40 kHz through a data acquisition module (NI DAQPad® 6015).

The optical system consisted of an infrared laser diode (Laser Components UK, PL15D060100A-0-0-01 wavelength 1.55µm, 5mW-CW, 100mA), coupled to an optic fiber with 9.2µm core diameter. A second Keithley 6221 current source provided currents up to 100 mA to the laser diode. The measured corresponding optical fiber output power levels increased almost linearly from 0 to 5mW, for currents between 40 mA and 100 mA. The underlying motive behind this setupis that by eventually using one or several laser beams in the infrared region it would be possible to heat the nerve very selectively (spatially and radially) and thus to achieve very localized, or "focused" temperature alterations. The absorption length of water is ~1mm for the wavelength 1.5µm [42].

Biological model. Ex vivo studies were conducted on the isolated Xenopus laevis sciatic nerves, as it is a well characterized and robust model. After dissection the nerve was carefully extracted, tied at both ends and immersed in amphibian Ringer's solution.

Experimental protocol. The stimulation current amplitudes for nerve activation were increased from 120µA to 230µA in steps of 10µA. Square pulses (300µs duration) were delivered at 1Hz for 5s at each current step. This stimulation sequence was repeated at each optical power. The optical power was regulated by laser diode current. The thermal equilibrium was virtually reached in a few hundreds of milliseconds for each laser power value. The main protocol for laser illumination was a continuous illumination, one minute for each laser intensity (time needed to scan through complete electrical stimulation sequence). The laser diode current was increased from 40mA to 100mA (in steps of 10mA) and then decreased from 100mA to 40mA and then to zero in order to detect any effects due to nerve fatigue or damage due to laser exposure (the non-monotonic nature of bipolar electrode thresholds was extensively studied in [43]). An additional protocol was used in order to confirm the heat block: intermittent illumination – the laser was switched on (to max current 100mA – power of 5mW) for 10s and then off for one minute. The sequence was repeated as OFF-ON-OFF-ON-OFF (with electrical stimulation sweep during each period).

IV. RESULTS

A. AP generation and propagation

Fig. 4a shows AP generation and propagation along the axon as obtained by our simulation technique. The time dependent extracellular potentials (created by the stimulus current shown in Fig.3b) just above nodes N20, N21 and N22 are also shown in Fig.4a. The AP is first generated at N20 and then propagates to both sides – only results for one side are shown due to the symmetry of the system.

The linear relationship between the conduction velocity and fiber diameter in single myelinated nerve fibers from

Xenopus laevis, with the slope of approximately 2 (m/s)/μm [44], was used to fit the value for the axial resistivity R_a. The

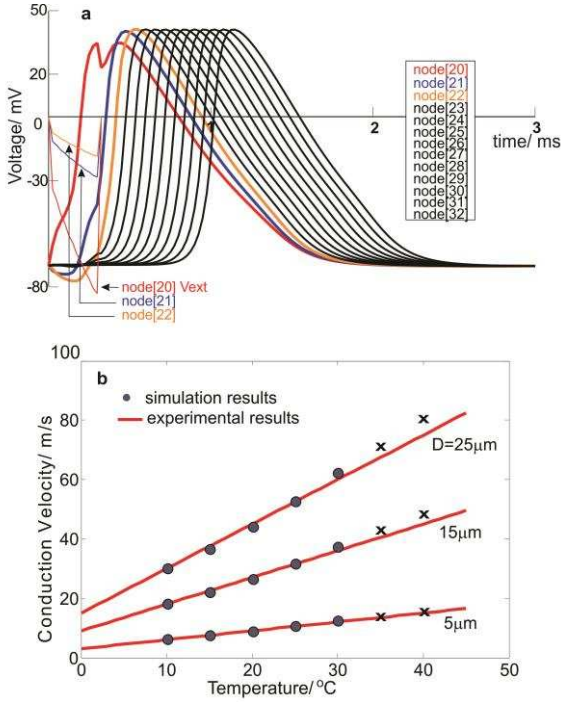

Fig. 4. Model tests: (a) AP generation, D = 15 μm, T = 23°C, stimulus pulse duration = 300 μs, stimulation current 147 μA, cathode above N20. Thin lines show the extracellular voltage at nodes 20-22 for constant current stimulation (comp. Fig. 3). (b) Conduction velocity vs. global temperature, the linear fit for the theoretical results is good for the temperature range 10–30°C, however a quadratic fit might be better outside that range (marked by x) for D>10μm. The conduction velocity of AP vs. fiber diameter was used for the model tests and adjustment of ρ_a by fitting to the experimental values from [44].

model also fits well the relationship between the conduction velocity θ [m/s] and temperature T [°C] in fibers of various diameters D [μm], Fig.4b. Hutchinson et.al [44] empirically established the relationship: θ = D (0.06T+0.6) (the red lines in Fig.4b), for the temperature range 15-30 °C. For our simulation data (circles, Fig.4b) both linear and quadratic fits are very close to the experimental data in the 15-30°C range. However, outside that range the simulation data could be better fitted by a quadratic relationship for thicker fibers (D>10μm). This type of exponential-like relationship was also observed by Moore [39]. All values for the conduction velocity scaled by the fiber diameter (θ/D) fall on a single universal curve in our model, approximately given by: θ/D = $0.008T^2 + 0.032T + 0.8$. For a linear fit in the range 10–30°C we get: θ/D = 0.064T + 0.52, very close to the result in [44].

The standard temperature for the FH node model is 20°C. The Q10 values used in our model are shown in Table 3. The axoplasm resistivity (ρ_a) strongly influences the impulse conduction velocity, and as it depends on temperature, in the present model we introduce Q10 value of $(1.3)^{-1}$ for ρ_a [39]. We also use a Q10 of 1.4 for the ionic conductances [39].

B. Selective electrical excitation and block

The excitation threshold will depend on the fiber diameter and its position in respect to the electrodes [45]. Two axial alignments were analysed: maximal alignment between the central node and the central electrode contact – cases (1) and (2) in Fig.5a), and maximal misalignment – cases (3) and (4). They include the nearest (r= R) and furthest (r= 0) positions of a fibre from the stimulation electrodes. These four cases cover the minimum and maximum stimulations needed to activate a fiber of an arbitrary diameter.

The threshold of neural activation is approximately inversely proportional to the square root of fiber diameter ($I_{thresh} \sim 1/\sqrt{D}$), as was previously shown in [22] and [32]. However, this relationship is strictly true only if the activation node is under the cathode (case (1) and (2) in Fig.5a,b). Results in Fig.5b show that for the positions (3) and (4) this relationship is not monotonic and exhibits a minimum value for a certain fiber diameter D, which depends on the distance between the electrodes. The reason is that the internode distance is assumed to be L ≈ 100 D hence the positions of N20 and N21 move in the external electric field as D changes and for certain position the internal potential difference between nodes N20 and N21 is maximal and the threshold stimulation current is minimal.

The smallest field is required for the thickest fiber at the border of the bundle when the cathode is just above a node, Fig.5b, case (1). The threshold increases for smaller fibers (case 1 and 2). So it is feasible to selectively activate specific types of fibers by choosing proper stimulus current but only of sufficiently high diameters and for specific positions of the nodes in respect to the electrodes.

The graph of the threshold stimulus strength (I_{thresh}) vs. stimulus duration (τ), the strength-duration curve, produced

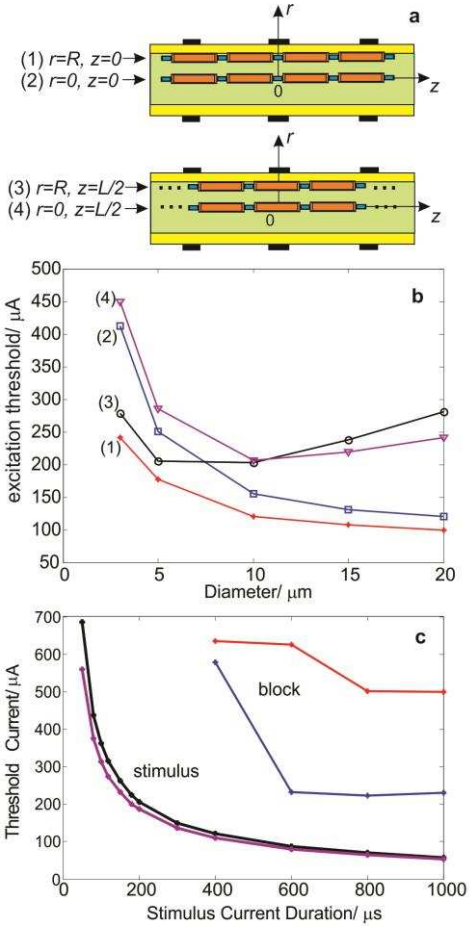

Fig. 5. Simulation results for selective electrical excitation/block. (a) Four characteristic cases for the positions (r,z) of the AP generating node (N20) in respect to the electrodes: (1) (R,0), (2) (0,0), (3) (R,L/2,) and (4) (0,L/2). (b) Minimum stimulus current of a 300μs pulse for activating a fiber as a function of the fiber diameter and position, for positions defined in (a).
(c) Stimulation/block threshold vs stimulus pulse duration: excitation of D=15μm (black) and D=25μm (purple) diameter fibers in the middle of the nerve bundle, i.e. position (2). The blocking threshold for fiber position (2) D=25μm (blue line) and for fiber position (1) D=15μm (red).

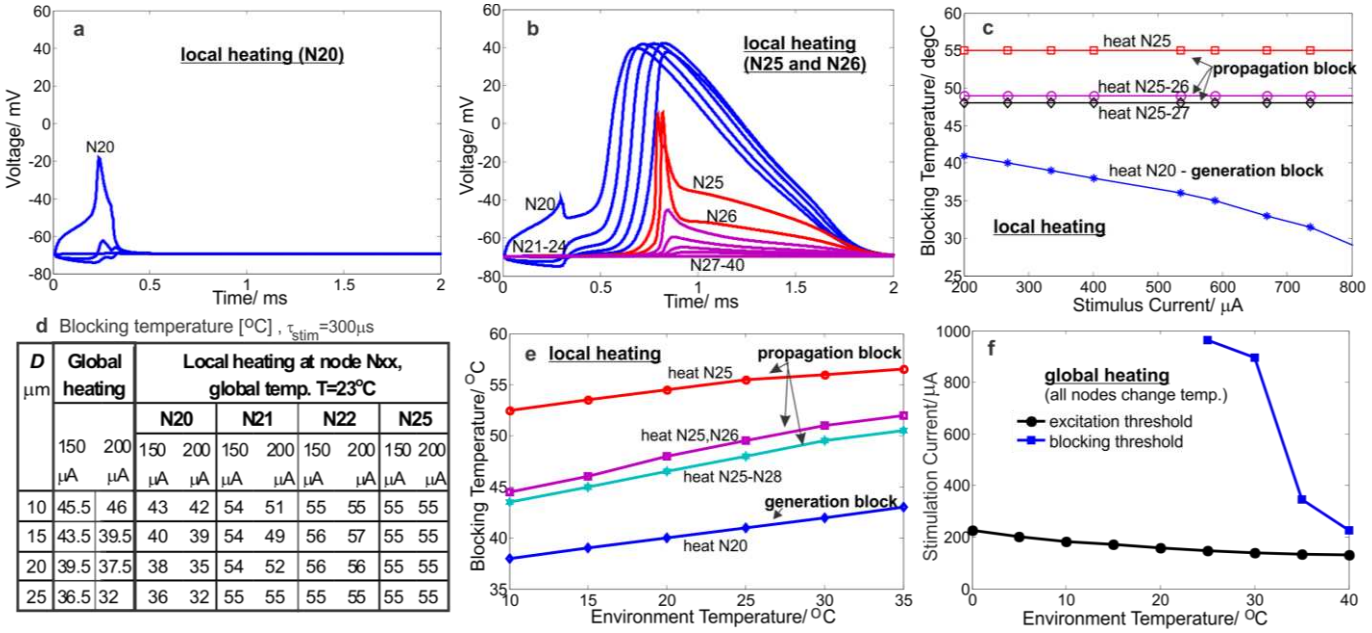

d Blocking temperature [°C] , τ_{stim}=300μs

D μm	Global heating		Local heating at node Nxx, global temp. T=23°C							
			N20		N21		N22		N25	
	150 μA	200 μA	150 μA	200 μA	150 μA	200 μA	150 μA	200 μA	150 μA	200 μA
10	45.5	46	43	42	54	51	55	55	55	55
15	43.5	39.5	40	39	54	49	56	57	55	55
20	39.5	37.5	38	35	54	52	56	56	55	55
25	36.5	32	36	32	55	55	55	55	55	55

Fig. 6. Simulation results: Heat block for a fiber in the middle of the nerve – position (2), D=15μm, the stimulus current is 200μA, pulse duration τ=300μs, all nodes not heated are at the environment temperature (which is T=23 °C for panels a,b and c). (a) The AP generation block: temperature of N20 (the AP generation node) is 40°C. Since the AP generation was blocked, all nodes are almost unaffected apart from a small spikelet at N20. (b) AP propagation block: the AP which propagated through the nodes N20-N24 (blue lines) blocked due to increased temperature (T= 49°C) of the nodes N25 and N26 (red). Violet lines are the membrane potential of the nodes N27-N40. The AP diminishes in nodes N27 to N40. (c) Minimum temperatures for the generation and propagation block vs. stimulus current. (d) Table of the blocking temperatures for both global and local temperature change, for various fiber diameters D in position (1). (e)The effect of the environment temperature on the blocking temperatures. (f) Electrical excitation and block vs. environment temperature.

by our model is shown in Fig.5c. It has a hyperbolic shape, as expected [46]. It is also possible to selectively block a fiber with sufficiently strong stimulus current ("electric block"), as shown in Fig. 5c. The fiber position and diameter again plays a crucial role. Clearly if electrical stimulation is used to, for example, selectively block the large fibers while activating thin fibers, it is important to ensure that the block of thin fibers in the vicinity of the electrodes is avoided. These results further demonstrate that electrical stimulation can be insufficient for selective neural inhibition, while making a strong case for the consideration of combined (electrical and heat) stimulation as an improvement.

C. Combined electrical and heat stimulus: Heat Block

An interesting question is what would be the dynamics of AP generation and propagation in myelinated axons if we had the ability to selectively change the temperature of certain nodes or myelinated sections of an axon. Using our model, we found that when the two inputs are combined, a local temperature increase can efficiently block APs – the so-called heat block. We identified two kinds of blocking: generation block and propagation block, depending on where the block occurs.

Generation blocking occurs when the node beneath the cathode (N20) is heated and fails to initiate a spike (in N21 and further) under suprathreshold electrical stimulation, see Fig.6a. The propagation block refers to the situation when one or several of the propagation nodes (N21-N40 in our case) are heated and an incoming action potential is arrested. Fig.6b shows the propagation block when N25 and N26 are heated. The generation block can be achieved for lower temperatures than the propagation block and the blocking temperature depends on the stimulus current (Fig.6c) and fiber diameter (Fig.6d-table). Higher stimulus currents or larger fiber diameters allow for lower blocking temperatures. The propagation block seems to be independent of the stimulus current amplitude – this is expected as the AP arrives at these nodes after the external stimulus pulse is terminated. The propagation block temperature for a single node (e.g. N22) and further down the axon (e.g. N25 shown in Table 6d) is virtually constant (approximately 55°C) and independent of D. N21 case shows lower temperatures than N22 and small variations with D. The propagation block temperature can be reduced by heating several nodes, e.g. N25-27 in Fig.6c.

In situations when the two inputs create a block, in order to restore AP propagation, one can either hold temperature constant and decrease stimulus current (Fig.6c), or hold electrical current constant and lower temperature (Fig.6f).

Fig. 6e shows that both generation and propagation block temperatures increase as the environment temperature increases (all nodes have this temperature if not heated), but the coefficient of proportionality is approximately only 0.2. The environment temperature has a strong effect on the electrical block threshold while the electrical stimulation threshold is much less affected (Fig.6f).

D. Experimental verification of the thermal block

The effect of temperature was investigated for the threshold activation, i.e. minimal electrical stimulation current needed to produce a nerve response (see Appendix D). In this way we avoided stimulation conditions leading to electrical block, and not to interfere with the characterization of thermal effects on the nerve. Furthermore, our theoretical predictions showed that "thicker" fibers are first activated at low stimulation currents (Fig.5b) but also these fibers are affected by lower temperatures at the AP generation node (about 35°C) than the thinner ones. The experimental value for the threshold electrical stimulation current ($\lesssim$150μA, Fig.7) is in good agreement with the simulation data shown in Fig.5b.

As shown in Fig.7 higher laser power (i.e. more energy dissipated in the nerve and higher temperature increase of some nodes) caused the need for higher stimulus current in

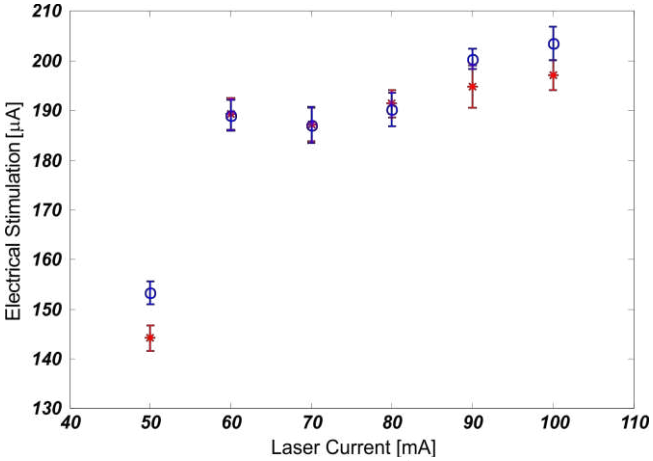

Fig.7. Experimental results: Average values for the electrical stimulation activation threshold vs. laser output power (i.e. diode currents), when the laser diode current increases (red asterix) and decreases (blue open circles). Laser threshold current is near 50mA and the maximum output power at the optical fiber (5mW) corresponds to the laser current of 100mA. Bars represent standard deviation, typically for 5-6 measurements. Measurements for both ascending and descending temperatures (laser currents/powers) are shown so that any effects due to nerve fatigue or damage can be seen. See Appendix D for further explanation. In experiments we used nerves from two frogs, here are displayed results for one nerve.

order to create recordable Compound Action Potentials (CAP). This phenomenon is in agreement with our simulation data in Fig.6 which suggested that if the AP generation node was heated, then the increase of local temperature at the node may block the creation of the AP. Our assumption is that the effect of the laser radiation is only due to the temperature increase caused by the absorption of the laser light.

V. Discussion

A model implemented in COMSOL and NEURON was created to simulate the thermoelectric extracellular stimulation of a myelinated nerve fiber. Both thermal and electrical effects were considered. We successfully managed to export and import information between the two simulation environments. The electrode-electrolyte interface was included and both the local and global temperature effects on the physical properties of the nerve were considered. The simulation data are in a good agreement with the experimental data, for example for predicting the minimum stimulation currents, etc. Hence we have created a tool which can simulate many different stimulation scenarios and it can help in optimizing the dimensions of the cuff electrodes and choosing appropriate signals for nerve excitation or block.

The model also allowed us to analyze the combined effects of the thermo-electric stimulation to the nerve. Lower environment temperatures required higher stimulus currents to excite or block the AP. Also, localized heating of the neural membrane (a few nodes) showed blocking of AP generation and propagation. For example, a fiber of D = 20 μm required minimum temperatures in the range of 30°C-40°C (at the node where the AP is generated) for the generation block. This temperature range should be physiologically acceptable and non-damaging for the frog's nerve, which has a typical operational temperature of ~20°C. But for the propagation block the required temperature is, according to our model, well above 50°C which is probably less physiologically acceptable and more damaging for the nerve [47].

Our experiments support these findings, as we demonstrated that when local temperature increases, the threshold for electrical activation increases for CAP generation. We interpret this effect as the local heat block of a fraction of the total number of fibers normally activated with solely electrical stimulation. Hence if some fibers are blocked, more fibers need to be activated in order to achieve a sufficiently strong neural activation to be recorded by our system. This can be achieved by increasing the stimulation current to reach out for more fibers within the nerve bundle which due to their position or diameter were not activated by the original stimulus (as shown in Fig.5b). We note here that increase of the stimulation amplitude will not reactivate the thermally blocked fibres (see Fig.6d), on the contrary, with increase of the stimulus current the blocking temperature decreases (Fig.6c) and even more fibers will be blocked. Also note here that the temperature increase will reduce the AP amplitude [10], but this will not affect the recorded signal because the recording cuff is placed at the part of the nerve which is not affected by the local heating process and Fig.8 below shows how APs amplitude recovers.

The mechanism for the transient heat block in the case of global heating and temperature change was proposed by Huxley [2] and further elaborated by Rattay and Aberham [3]. With increase of temperature, change of the gating variables and the ion channel permeability are accelerated (Appendix A, eq.(2)-(4) and values for Q_{10} in Table III). However, acceleration or the raising phase of the AP is gradually overpowered by the acceleration of the sodium channels inactivation and potassium channels activation and eventually for some temperature the positive feedback is suppressed and an AP cannot be formed. Similar mechanisms apply to local heating and the generation block, since in that case the AP initiation in the axon is blocked. In the case when the AP is already initiated and starts to "jump" from node to node, then ion channel gating kinetics becomes less important. If only one (or a few) nodes are heated the AP can get through them and recover in the nodes downstream, Fig.8. Hence much higher temperatures for the propagation block are needed, but the axonal dynamics becomes more import as shown below.

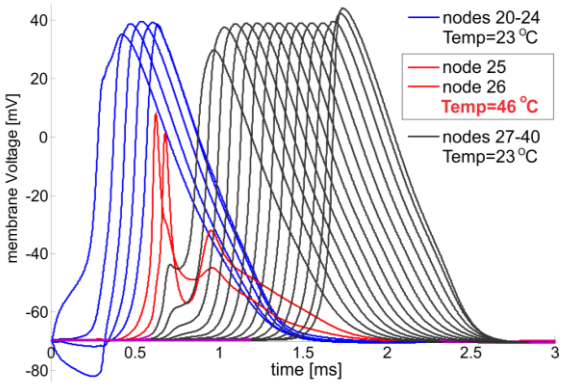

Fig. 8. AP can get through certain number of nodes at high temperature. A proportion of channels at hot nodes (here N25 and N26) are still excitable to a given level of depolarization and will open allowing a small current to traverse a region of relative inexcitability. Once that region is passed, the current will induce a larger depolarization in the cooler regions (N27-N40), as the channels remain open longer, reestablishing a measurable AP.

The effects of the axonal dynamics, specifically the axoplasm resistivity ρ_a, on the heat block can be analysed using results in Table IV. As the resistivity increases there is a small drop of the blocking temperature (T_{block}) for global heating and almost no change for local heating at the node of

AP generation. However there is a significant reduction of T_{block} for the propagation block (N21-23) which can be explained by drop of the axonal depolarisation current between the nodes due to increased axoplasm resistance.

TABLE IV
EFFECT OF AXOPLASM RESISTIVITY (ρ_A) ON THE BLOCKING TEMPERATURE

ρ_a [Ω·cm]	D [μm]	Global heating	Local heating at node Nxx, AP generated at N20, global temperature T=23°C			
		150/200μA	N20	N21	N22	N25
			150/200μA	150/200	150/200	150/200
65	20	39.5/37.5°C	38/35 °C	54/52 °C	56/56 °C	55/55 °C
100	20	38.5/36 °C	38.5/34.5	50/48.5	50.5/50.5	50/50

In our experiments all thermal effects are very local since the global temperature of the solution, measured near the recording cuff, did not change during the experiments. The amount of energy absorbed in the bath at the maximum laser power is 5mW, therefore overall average increase of temperature in the water solution would be less than 0.01°C for 30 minutes of continuous laser operation (in each experiment the laser was On for less than 15 minutes in total). However, since the laser light was coupled to a fiber of about 10μm diameter, the diameter of the assumed Gaussian profile of the laser beam inside the nerve was increasing from about 60μm to 300μm on the other end. Now if no cooling were to occur due to thermal conduction in water, the temperature inside this truncated cone of water would on average increase for 30°C after one second of laser illumination. However, simulations of heat diffusion in water and cylindrical geometry (results not shown) suggest that thermal conduction of water is enough to limit any excessive rise of temperature and transitional periods are very short (<100ms) for maximum laser power of 5mW. More accurate theoretical predictions would consider different thermal conductivities of water and myelin and consequently an anisotropic geometry with elongated cylindrical fibers. Our rough estimates, based on computer simulations of water heating and heat dissipation in Matlab, suggest that the local temperature increase of about 10°C is possible in our system (see Appendix C for details).

Results of several experimental studies of the near infrared illumination of neural tissue give similar results, such as infrared camera recordings of nerve tissue heated by a laser light [18] and NIR light beam pulsed into a rat brain [48]). This level of temperature increase at the AP generation node is enough for the transient heat block of the thickest fibers in the frog's sciatic nerve (D≥20μm, Fig.6d).

At first glance, these results seem to be in disagreement with the now well-established technique of neural excitation using IR lasers [14, 17-18, 49]. However, the major difference is that in the case of excitation, very short pulses of very powerful lasers were used over a larger area of nerve bundle (e.g. power density of ~10W/mm^2 for 2ms, using 400μm fiber [35]) whereas in our case the laser power is much lower (power density less than 1W/mm^2 at the area of diameter ~100μm), but applied for much longer duration.

VI. CONCLUSION

This work demonstrated that by using localized temperature increase of nodes the transient heat block is possible. The required temperatures for AP generation block seem physiologically safe. Therefore it should be possible to achieve selective activation or inhibition of neural activity by applying focused infra-red light to selectively block specific fibers in a nerve bundle whilst using electrical stimulation to activate some other fibers. Selective stimulation has important therapeutic applications and this strategy might be primarily applicable to peripheral nerve interfacing. The technique will offer spatial selectivity and would be a novel method for addressing individual neural pathways in densely populated nerve groups, such as major peripheral nerves. This work presents a proof-of-concept investigation, but further work on geometric optimization (both experimentally and theoretically) is necessary to fully realize a functional interface for selective nerve stimulation. The model files are available upon request and on the last author's web site.

VII. APPENDIX

A. The Axon model equations

The ionic current per unit area in eq.(1) is given by the FH model and represents the sum of sodium, potassium, non-specific and leak currents [19]:

$$i_{ion} = i_{Na} + i_K + i_p + i_L \qquad (2)$$

$$i_{Na} = \phi_{ch}\overline{P_{Na}}\square\square\square m^2 h\square\square\square\square\square\square\frac{UF^2}{RT}\frac{[Na]_{ext} - [Na]_{int}\exp(UF/RT)}{1 - \square\square\square\exp(UF/RT)}$$

$$i_K = \phi_{ch}\overline{P_K} n^2 \frac{UF^2}{RT}\frac{[K]_{ext} - [K]_{int}\exp(UF/RT)}{1 - \exp(UF/RT)}$$

$$i_p = \phi_{ch}\overline{P_p} p^2 \frac{UF^2}{RT}\frac{[Na]_{ext} - [Na]_{int}\exp(UF/RT)}{1 - \exp(UF/RT)}$$

$$i_L = \phi_{ch}\, g_L(V - E_L)\,.$$

Values for the ionic permeabilities ($\bar{P}$), ionic concentrations, leak conductance (g_L) and reversal voltage (E_L) are given in Table III. F is the Faraday's constant and R is the universal gas constant and T is the absolute temperature. The gating variable m is modeled by:

$$\frac{dm}{dt} = \phi_m \cdot [\alpha_m(1 - m) - \beta_m m] \qquad (3)$$

ϕ_m is a thermic coefficient which depends on the difference between the actual temperature T and a referent temperature T_0 and a special constant Q_{10} introduced by Hodgkin and Huxley which describes the acceleration in the membrane kinetics when the temperature is increased by 10 °C:

$$\phi_m = Q_{10,m}^{(T-T_0)/10} \qquad (4)$$

In our model, not only membrane kinetics was affected by temperature, but channel permeabilities ($\bar{P}$) as well, hence a similar factor to (4) was introduced for ionic currents:

$$\phi_{ch} = Q_{10,ch}^{(T-T_0)/10}\,.$$

Similar expression to (3) is for h. αs and βs are given by:

$$\alpha_m = A(V - B)/[1 - \exp((B - V)/C)] \qquad (5)$$

$$\beta_m = A(B - V)/[1 - \exp((V - B)/C)] \qquad (6)$$

$$\alpha_h = A(B - V)/[1 - \exp((V - B)/C)] \qquad (7)$$

$$\beta_h = A/[1 + \exp((B - V)/C)] \qquad (8)$$

Gating variables n and p are modeled by equivalent set of equations to (4)–(8). Values for Q_{10} are in Table III. The values for As, Bs and Cs for m, h, n and p are given in [20].

Each myelin section was divided into ten segments and modelled as passive section: $g_L = g_{myelin} = 1.5\cdot 10^{-5}/D$ S/cm^2 and $c_m = c_{myelin} = 0.157/(\pi D)$ μF/cm^2. The axoplasm conductance

between two nodes is: $G_a = \pi d^2/(4\rho_a L) = 0.00385 \cdot D/\rho_a$, where D and ρ_a are defined in Table III, including Q10 value for ρ_a.

B. COMSOL boundary conditions

The boundaries of the area considered in the simulations are at r=10mm, z= -56mm and z=56mm, see Fig.9. Zero current was assumed to flow across that boundary ($\mathbf{n}\cdot\mathbf{J}=0$), i.e. the boundary beyond the compartment marked Saline is assumed to be insulating. The system has axial symmetry around the middle line of the nerve bundle, where r=0. The electric current is continuous across the internal boundary between the nerve (rectangle N, current at the boundary is $\mathbf{J}_1$) and saline (rectangle Saline, $\mathbf{J}_2$): hence for the normal components of the currents holds $\mathbf{n}\cdot(\mathbf{J}_1-\mathbf{J}_2)=0$.

B1, B2, B3 and B4 in Fig. 9 are electric shielding with d=10μm thickness. The electric shielding describes a thin layer of a dielectric medium using tangential derivative:

$$\mathbf{n}\cdot(\mathbf{J}_1-\mathbf{J}_2) = -\nabla_t\, d(\sigma\nabla_t V + \varepsilon_0\varepsilon_r\,\partial(\nabla_t V)/\partial t)\,,$$

where σ is the cuff electric conductivity and ε_r relative permittivity. A1 and A2 are taken to be at Ground (V=0), while C is defined as Port. The stimulus current is added to C.

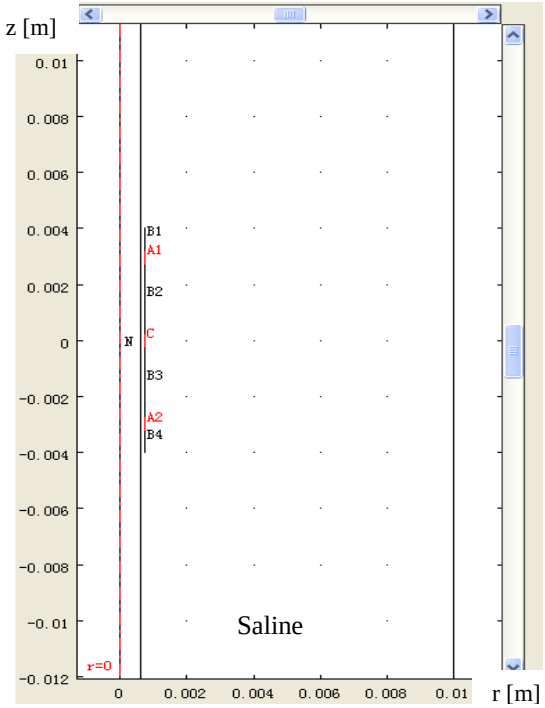

Fig 9. Geometry of the system in COMSOL used to define the boundary conditions. N is the nerve bundle rectangle and Saline is the saline solution rectangle. A1, A2, B1, B2, B3, B4 and C are described in the text.

C. Water heating with a laser beam

Water is heated due to the absorption of IR light and the heat is dissipated due to heat conduction through water. We assume that that these are the only two mechanisms affecting the water temperature (T). The water temperature change, at time t and at the point (ρ, ξ) may be described:

$$\frac{\partial T}{\partial t} = D\cdot\Delta T + B\cdot I(\rho,\xi)$$

where ρ is the distance from the fibre tip along the beam axis and ξ is the distance from the axis in perpendicular direction (axial symmetry is assumed). Here D is the "diffusion" constant, D= k/(σc), where k is the thermal conductivity, c the specific heat capacity and σ the density of water. B= α/(σc), where α is the coefficient of absorption of electromagnetic radiation in water for a specific wavelength (for λ=1.55μm α ~1mm^{-1}). When the beam leaves the fiber it begins to spread and can be represented as a fundamental Gaussian beam:

$$I(\rho,\xi) = I_0(\xi)\, e^{-\rho^2/(2w^2)}\,,\; w = w_0\sqrt{1+[\lambda\xi/(\pi w_0^2)]^2}$$

where $I_0(\xi) = (P_0/(2\pi w_0^2))\cdot\exp(-\alpha\xi)$, and P_0 is the output laser power at the fiber end. In our case P_0 is between zero and 5mW and initial beam radius is w_0=4.6μm.

D. Experimental results

Fig.10 shows a small selection of experimental results. Panel (a) describes the procedure of identifying the threshold of electrical stimulation current for the result shown in Fig.7. Panel (b) shows how a stronger electrical stimulation is needed in order to evoke the same neural response as the laser intensity increases.

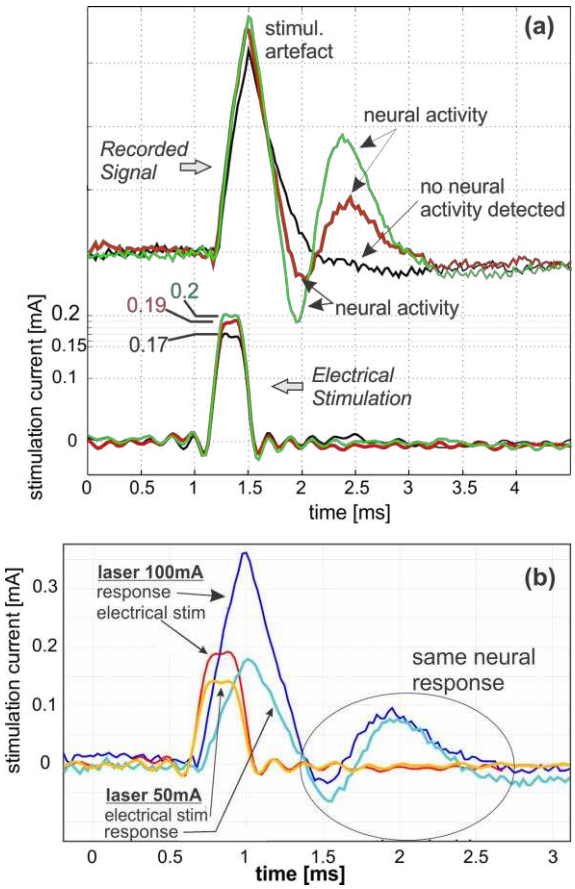

Fig. 10. (a) Activation Threshold: the values for the electrical stimulation were increased in steps of 10μA (only lines for 0.17mA (black), 0.19mA (red) and 0.2mA (green) are shown) and the threshold for the neural activation registered by the recording cuff electrodes shown in Fig.1d is the minimum stimulation when the characteristic signal shape for the CAP emerges [36] – red line. A detailed model for the produced CAC and CAP by a nerve bundle was given in [36]. (b) Electrical stimulation currents for laser powers 50mA and 100mA (orange and red lines respectively) and threshold response (circled) – trace for laser-100 has a small vertical offset for clarity.

REFERENCES

1. Navarro, X., et al., A critical review of interfaces with the peripheral nervous system for the control of neuroprostheses and hybrid bionic systems. J Peripheral Nerv Sys, 2005. **10**(3): p. 229-258.
2. Boger, A., N. Bhadra, and K. Gustafson, Bladder voiding by combined high frequency electrical pudendal nerve block and sacral root stimulation. Neurourol Urodyn, 2008. **27**(5): p. 435-9.
3. Ackermann, D.M., et al., Nerve conduction block using combined thermoelectric cooling and high frequency electrical stimulation. J. Neurosci. Meth., 2010. **193**(1): p. 72-76.
4. Ackermann, D.M., et al., Conduction Block of Peripheral Nerve Using High Frequency Alternating Currents Delivered through an Intrafascicular Electrode. Muscle Nerve, 2010. **41**(1): p. 117-119.

5. Bhadra, N. and K.L. Kilgore, Direct current electrical conduction block of peripheral nerve. Neural Systems and Rehabilitation Engineering, IEEE Transactions on, 2004. **12**(3): p. 313-324.
6. Kilgore, K.L. and N. Bhadra, Nerve conduction block utilising high-frequency alternating current. Med Biol Eng Comput, 2004. **42**(3): p. 394-406.
7. Joseph, L. and R.J. Butera, High-Frequency Stimulation Selectively Blocks Different Types of Fibers in Frog Sciatic Nerve. Neural Systems and Rehabilitation Engineering, IEEE Transactions on, 2011. **19**(5): p. 550-557.
8. Gerges, M., et al., Frequency- and amplitude-transitioned waveforms mitigate the onset response in high-frequency nerve block. J. Neural. Eng., 2010. **7**(6): p. 066003.
9. Hodgkin, A.L. and B. Katz, The Effect of Temperature on the Electrical Activity of the Gian Axon of the Squid. J. Physiol., 1949. **109**: p. 240-9.
10. Huxley, A.F., Ion movements during nerve activity. Ann. NY Acad. Sci., 1959. **81**(2): p. 221-246.
11. Rasminsky, M., The Effects of Temperature on Conduction in Demyelinated Single Nerve Fibers. Arch Neurol, 1973. **28**(5): p. 287-292.
12. Klumpp, D. and M. Zimmermann, Irreversible Differential Block of A- and C-fibres Following Local Nerve Heating in the Cat. J. Physiol., 1980. **298**: p. 471-482.
13. Rattay, F. and M. Aberham, Modeling Axon Membranes for Functional Electrical Stimulation. IEEE Trans. Biomed. Eng., 1993. **40**(12): p. 1201-1209.
14. Wells, J., et al., Application of infrared light for in vivo neural stimulation. J. Biomed. Opt., 2005. **10**(6): p. 064003-12.
15. Wells, J., et al., Optical stimulation of neural tissue in vivo. Opt. Lett., 2005. **30**(5): p. 504–507.
16. Teudt, I.U., et al., Optical Stimulation of the Facial Nerve: A New Monitoring Technique? The Laryngoscope, 2007. **117**(9): p. 1641-47.
17. Izzo, A.D., et al., Laser stimulation of the auditory nerve. Laser Surg. Med., 2006. **38**(8): p. 745-753.
18. Wells, J., et al., Biophysical Mechanisms of Transient Optical Stimulation of Peripheral Nerve. Biophys. J., 2007. **93**(7): p. 2567-2580.
19. Frankenhaeuser, B. and A.F. Huxley, The action potential in the myelinated nerve fibre of Xenopus laevis as computed on the basis of voltage clamp data. J. Physiol., 1964. **171**(2): p. 302-315.
20. Butikofer, R. and P.D. Lawrence, Electrocutaneous Nerve Stimulation-I: Model and Experiment. IEEE Trans. Biomed. Eng, 1978. **BME-25**(6): p. 526-531.
21. Dean, D. and P.D. Lawrence, Application of Phase Analysis of the Frankenhaeuser - Huxley Equations to Determine Threshold Stimulus Amplitudes. IEEE Trans. Biomed. Eng., 1983. **30**(12): p. 810-818.
22. McNeal, D.R., Analysis of a Model for Excitation of Myelinated Nerve. IEEE Trans. Biomed. Eng., 1976. **23**(4): p. 329-337.
23. Fitzhugh, R., Computation of Impulse Initiation and Saltatory Conduction in a Myelinated Nerve Fiber. Biophys. J., 1962. **2**(1): p. 11-21.
24. Bostock, H., The strength-duration relationship for excitation of myelinated nerve: computed dependence on membrane parameters. J. Physiol., 1983. **341**(1): p. 59-74.
25. Rattay, F., Analysis of Models for Extracellular Fiber Stimulation. IEEE Trans. Biomed. Eng., 1989. **36**(7): p. 676-682.
26. Carnevale, N.T. and M.L. Hines, The NEURON book. 2006: Cambridge Univ Press.
27. Martinek, J., et al., A Novel Approach to Simulate Hodgkin-Huxley-like Excitation With COMSOL Multiphysics. Artificial Organs, 2008. **32**(8): p. 614-619.
28. Schiefer, M.A., R.J. Triolo, and D.J. Tyler, A Model of Selective Activation of the Femoral Nerve With a Flat Interface Nerve Electrode for a Lower Extremity Neuroprosthesis. IEEE Trans Neural Sys & Rehabil Eng, 2008. **16**(2): p. 195-204.
29. Zarifi, M.H., et al., Finite-element analysis of platinum-based cone microelectrodes for implantable neural recording, in 4th Int. Conf. IEEE EMBS Neural Eng. 2009, IEEE: Antalya, Turkey. p. 395-398.
30. Raspopovic, S., et al., Comparison of intraneural electrode geometries: Preliminary guidelines for electrode design, in 4th Ann. Int. Conf. IEEE EMBS Neural Eng. 2009, IEEE: Antaly, Turkey. p. 64-67.
31. Jacquir, S., et al. Computation of the electrical potential inside the nerve induced by an electrical stimulus. in 29th Conf IEEE EMBS. 2007.
32. Goodall, E.V., et al., Modeling Study of Activation and Propagation Delays During Stimulation of Peripheral Nerve Fibers with a Tripolar Cuff Electrode. IEEE Trans. Rehabil. Eng., 1995. **3**(3): p. 272-282.
33. Woods, V., I. Triantis, and C. Toumazou, Offset prediction for charge-balanced stimulus waveforms. J. Neural Eng., 2011. **8**: p. 046032.
34. Frankenhaeuser, B. and L.E. Moore, The effect of temperature on the sodium and potassium permeability changes in myelinated nerve fibres of Xenopus laevis. J. Physiol., 1963. **169**(2): p. 431-437.
35. Hines, M., Xenopus Myelinated Neuron, Frankenh. & Huxley 1964. Coded in NEURON: http://senselab.med.yale.edu/modeldb (3507).
36. Wijesinghe, R., F. Gielen, and J. Wikswo, A model for compound action potentials and currents in a nerve bundle I: The forward calculation. Ann. Biomed. Eng., 1991. **19**(1): p. 43-72.
37. Goldman, L. and J.S. Albus, Computation of Impulse Conduction in Myelinated Fibers; Theoretical Basis of the Velocity-Diameter Relation. Biophys. J., 1968. **8**(5): p. 596-607.
38. Dodge, F.A. and B. Frankenhaeuser, Sodium currents in the myelinated nerve fibre of Xenopus laevis investigated with the voltage clamp technique. J. Physiol., 1959. **148**(1): p. 188-200.
39. Moore, J.W., et al., Simulations of conduction in uniform myelinated fibers. Relative sensitivity to changes in nodal and internodal parameters. Biophys. J., 1978. **21**(2): p. 147-160.
40. Zeng, S., Y. Tang, and P. Jung, Spiking synchronization of ion channel clusters on an axon. Phys. Rev. E, 2007. **76**(1): p. 011905.
41. Triantis, I., A. Demosthenous, and N. Donaldson, On Cuff Imbalance and Tripolar ENG Amplifier Configurations. IEEE Trans. Biomed. Eng., 2005. **52**: p. 314-320.
42. Curcio, J.A. and C.C. Petty, The Near Infrared Absorption Spectrum of Liquid Water. J. Opt. Soc. Am., 1951. **41**(5): p. 302-302.
43. Holsheimer, J. and W. Wesselink, Optimum electrode geometry for spinal cord stimulation: The narrow bipole and tripole. Med Biol Eng Comput, 1997. **35**(5): p. 493-497.
44. Hutchinson, N.A., Z.J. Koles, and R.S. Smith, Conduction velocity in myelinated nerve fibres of Xenopus laevis. J. Physiol., 1970. **208**(2): p. 279-289.
45. Warman, E.N., W.M. Grill, and D. Durand, Modeling the Effects of Electric Fields on Nerve Fibres: Determination of Excitation Thresholds. IEEE Trans. Biomed. Eng., 1992. **39**(12): p. 1244-1254.
46. Marghescu, D., The McGill Physiology Virtual Laboratory. 2011.
47. Duncan, C.J., Effect of lethal high temperature on isolated frog skeletal muscle. J. Therm. Biol., 1989. **14**(2): p. 95-98.
48. Abdo, A., A. Ersen, and M. Sahin. Temperature Elevation inside Neural Tissue Illuminated by NIR Laser. in 33rd Conf IEEE EMBS. 2011.
49. Duke, A.R., et al., Combined optical and electrical stimulation of neural tissue in vivo. J Biomed Optics Lett, 2009. **14**(6): p. 060501.

Zongxia Mou is with the Bioengineering College, Chongqing University, Chongqing 400044, China. She received the B.Eng. degree in Biomedical Engineering at China University of Mining and Technology, Jiangsu, China in 2006. She was a visiting student at Institute of Biomedical Engineering, Imperial College London from 15 Dec 2009 to 23 Dec 2010. Currently she is working toward her Ph.D. degree in Biomedical engineering at the University of Chongqing, Chongqing, China. Her interests include BioMEMS and neural electrical stimulation, especially in wireless implantable systems.

Iasonas F. Triantis is a Lecturer at City University, London UK. Previously he was a Senior Researcher in microelectronics for electrical impedance tomography at the Department of Electronic and Electrical Engineering, University College London. During his Ph.D. in the same department, and later as a Research Associate at Imperial College, he designed neural sensing and stimulation chips, and researched alternative neural interfacing methods.

Virginia M. Woods received a B.Sc. in Biological Engineering from Cornell University in 2006 and in 2012 she gained her PhD at Imperial College London Ph.D. in Neural Engineering. Her research focuses on the bioelectric design of stimulus waveforms for peripheral nerve activation.

Christofer Toumazou FRS, FREng, FIEEE, FIEE CEng is a Professor of Circuit Design and the Chief Scientist of the Institute of Biomedical Engineering at Imperial College London. His research interests include high-frequency analog integrated circuit design for RF electronics and low-power electronics for biomedical applications. Prof. Toumazou is a past Chairman for the Analog Signal Processing Committee and the past Vice President of Technical Activities for the IEEE Circuits and Systems (CAS) Society. He founded the IEEE BIOCAS Society in 2000. He is also the founder of technology-based companies with applications spanning ultra low-power mobile technology and wireless glucose monitors.

Konstantin Nikolic received the BEng and MSc from the Department of Electrical Engineering, Belgrade University, Serbia and the PhD in physics from Imperial College London, UK. He was an Associate Professor at the Faculty of Electrical Engineering, Belgrade University, then Senior Research Fellow at the Dep. of Physics & Astronomy, University College London and now he is Wilfred Corrigan Research Fellow at the Department of Electrical and Electronic Engineering, Imperial College London. His current research

interests include the computational neuroscience and mathematical modeling of various cellular signaling processes.